crystals

MDPI

Article

Development and Characterization of CrCoNi Medium Entropy Alloy Particles Reinforced Aluminum Matrix Composite

Yue Wu [1], Siwei Luo [1], Jiawei Wu [1], Baisong Guo [1,2,*], Zhenggang Wu [3], Biao Chen [4], Zhentao Yu [1,*], Zhiguo Zhang [1] and Wei Li [1]

[1] Institute of Advanced Wear & Corrosion Resistant and Functional Materials, Jinan University, Guangzhou 510632, China
[2] Department of Materials Science and Engineering, City University of Hong Kong, Kowloon Tong, Kowloon, Hong Kong, China
[3] College of Materials Science and Engineering, Hunan University, Changsha 410082, China
[4] State Key Laboratory of Solidification Processing, Northwestern Polytechnical University, Xi'an 710072, China
* Correspondence: guobaisong@jnu.edu.cn (B.G.); ninyzt@163.com (Z.Y.)

Abstract: As for metal matrix composites (MMCs), the selection and application of reinforcements play a vital role in their comprehensive properties. In this work, the CrCoNi medium entropy alloy (MEA) was selected as reinforcement for Al matrix composites, and the effects of the content of the CrCoNi MEA on the mechanical properties and friction resistance were systematically investigated. It was found that the CrCoNi MEA can effectively improve the mechanical properties of the Al matrix composites, especially the 5 wt.% CrCoNi/Al composite can achieve a high strength without the sacrifice of ductility, due to the strengthened interfacial bonding between the Al matrix and the CrCoNi reinforcements caused by the element interdiffusion and the high mechanical performance of the CrCoNi MEA itself. In addition, the wear resistance of the composites can be enhanced by the inclusion of the CrCoNi MEA reinforcement, because the CrCoNi MEA can substantially improve the hardness of the composites and promote the formation of the oxidative protection film during the friction process. This work paves a new route for preparing Al matrix composites with high mechanical properties and friction resistance.

Keywords: Al matrix composites; medium entropy alloy; mechanical properties; tribological properties

Citation: Wu, Y.; Luo, S.; Wu, J.; Guo, B.; Wu, Z.; Chen, B.; Yu, Z.; Zhang, Z.; Li, W. Development and Characterization of CrCoNi Medium Entropy Alloy Particles Reinforced Aluminum Matrix Composite. *Crystals* **2022**, *12*, 1452. https://doi.org/10.3390/cryst12101452

Academic Editor: Cyril Cayron

Received: 19 September 2022
Accepted: 11 October 2022
Published: 14 October 2022

1. Introduction

With the rapid development of science and technology, the application of metal matrix composites in industrial production has gradually increased, such as the Ti-based composites [1–6], the Cu-based composites [7–9], the Al-based composites [10], etc. Especially, aluminum matrix composites (AMCs) have been widely utilized as structural materials in aerospace, automotive, electronics and other industrial fields, due to their low density, high specific strength and specific modulus, good fatigue resistance and low coefficient of thermal expansion (CTE) [11–13]. Ceramic particles, such as SiC [14], $A1_2O_3$ [15] and B_4C [16] have a strong strengthening potential for the Al matrix, due to their intrinsically high strength, stiffness and wear resistance. However, they cannot form strong a metallurgy bonding interface with the Al matrix, owing to their chemical stability, these weak interfaces generally result in a low load transfer efficiency from the Al matrix to the reinforcements [17]. Moreover, hard ceramic particles are not easy to process, and prefer to be broken during the deformation, the broken ceramic particles can act as the crack sources [18]. The plastic deformation capacity and CTE of the ceramic particles is quite different from the Al matrix, the stress concentration and micro-crack nucleation tend to occur at the interface, thereby reducing the plasticity and fracture toughness of the prepared composites [19]. Therefore, it can be expected that selecting the appropriate reinforcements and improving the interface bonding between the reinforcements and

the matrix are effective attempts to improve the strength and deformation ability of the Al matrix composite [20–23].

In order to overcome the shortcomings of the ceramic particles for reinforcing the Al matrix composites, researchers have turned their attention to metal particle reinforcements, and attempted to achieve a good bonding interface with the help of the nature of the metal-metal bonding. Metallic glass can form a proper interfacial bonding with the metal matrix, but can also cause cracks in the nucleation and thus reduce the plasticity of the composite materials, due to its intrinsically low ductility [24]. In 2004, Ye et al. first proposed a new alloy design concept, i.e., a qui-molar or near-equimolar ratio of the multi-principal elements of high entropy alloys (HEAs) [25], which highly broaden the composition range of elements for designing alloys. HEAs contain at least five main elements, and the concentration of each element is 5–35%. In the concept of "high entropy" [26–28], the choice of a high mixing entropy and alloy composition makes the alloy system obtain a higher ΔS_{mix} when the multi-elements are mixed in equimolar fractions, which enable the alloy to produce a more stable solid solution instead of the intermetallic compounds, which facilitate achieving a strong metallurgical bonding with other metal matrices. Furthermore, it has been fully demonstrated that HEAs have an ultra-high strength and ductility, a good thermal stability, an excellent wear and corrosion resistance. Hence, the HEA has been regarded as a promising reinforcement for metal matrix composites, especially for Al matrix composites. For example, Liu et al. [29], fabricated 5 vol.% AlCoCrFeNi high-entropy alloy particle reinforced Al matrix composites by spark plasma sintering. A transition layer with the FCC structure is formed between the Al matrix and the reinforcement, which significantly improves the yield strength and the ductility of the composites. The compressive strength and the compressive strain were 137 MPa and 50%, respectively. Following the loading, there was no macroscopic fracture observed in the failed aluminum matrix composites. Li et al. [30], fabricated $Al_{0.8}$CoCrFeNi HEA particle-reinforced Al matrix composites through a multi-channel friction stir process. The yield strength and the ultimate tensile strength of the composites were increased by 42% and 22%, respectively, compared with the unreinforced Al matrix, without any sacrifice of the ductility. The interface diffusion that occurs in the interface region between the reinforcement and the Al matrix, forms the Al_3CoCrFeNi high entropy alloy instead of the intermetallic compounds.

Compared with high-entropy alloys, medium-entropy alloys with a lower configuration entropy have fewer elements, a lower stacking fault energy and a faster atomic diffusion rate, thus exhibiting different mechanical property features. Based on previous works [31–36], it has been further proved that only a small part of the multi-element equiatomic alloys can also reach a single-phase solid solution with high configuration entropies and increasing the types of elements cannot enhance the configuration entropy [37]. For example, the equal atomic ratios of only Cr, Co and Ni can form a single-phase solid solution with the FCC structure. In addition, it is demonstrated that the yield strength and the ultimate strength of the CrCoNi medium entropy alloy (MEA) increase rapidly with the decrease of temperature, and their physical and chemical properties are comparable to that of HEAs. Furthermore, Gludovatz et al. [38], used arc smelting to prepare the CrCoNi MEA alloy, and tested its mechanical properties at room temperature and at a low temperature, respectively. The results showed that the room temperature tensile strength was 1 GPa, the fracture strain was 70%, the fracture toughness was above 200 $MPam^{1/2}$, exhibiting a higher strength and fracture toughness at low temperatures, compared to HEAs. Moravcik et al. [39], utilized advanced powder metallurgy and spark plasma sintering technology to prepare the MEA, which fully demonstrated that the MEA can be used to fabricate composites and present similar properties to HEAs, while the cost is lower and the preparation is simpler. However, until now, there are few studies using the MEA as the reinforcement for preparing the Al matrix composites.

In this article, the Al matrix composites were prepared using powder metallurgy and the CrCoNi MEA as reinforcements, the fundamental relationship between the CrCoNi content and the mechanical properties and the tribological properties of the composites

was systematically investigated. The findings benefit the reinforcement selection and the microstructure regulation for developing the Al matrix composites with high mechanical properties and friction resistance.

2. Experimental

2.1. Fabrication of the Composites

The raw spherical Al powder (2 μm in average particle size) and the raw spherical CrCoNi powder (15 μm in average particle size, atomic ratio of 1:1:1) were used as the matrix and the reinforcement materials, respectively. First, the spherical Al powder was pre-milled into Al flakes via mechanical ball-milling for 3 h. The ball-milling speed was 300 rpm, and the ball to powder weight ratio was 8:1. During the milling process, Ar was employed as the protection gas. The flaky CrCoNi powder was obtained by ball-milling with the rotation speed of 400 rpm and the ball-to-powder weight ratio of 20:1, respectively. To ameliorate the cold welding during the ball-milling, 0.75 wt.% zinc stearate was added for pre-milling the Al and CrCoNi powders. Then the Al and CrCoNi flaky powders were mixed through a 3 h wet ball-milling process with absolute alcohol as the ball-milling medium. The milling speed was 300 rpm and the ball-to-powder weight ratio was 5:1. Following the wet-milling, the vacuum filtration and drying were utilized to completely remove the absolute alcohol. The dried composite powders were then transferred into the FHP-828 quick hot pressing sintering furnace and the sintering was carried out at 600 °C for 0.5 h in an argon atmosphere with a heating and cooling rate of 100 °C/min. During the whole sintering process, a mechanical pressure of 40 MPa was exerted on the sample to accelerate the densification of the specimens. In order to realize the full densification of the composites, these sintered samples (Φ 40 × 8 mm) were further hot rolled at 450 °C, and the thickness was reduced by 50%, through five passes. Four batches of the composite samples, reinforced with 5, 10, 15 and 20 wt.% CrCoNi particles were fabricated using the same process. The detailed preparation process of the composites is shown in Figure 1.

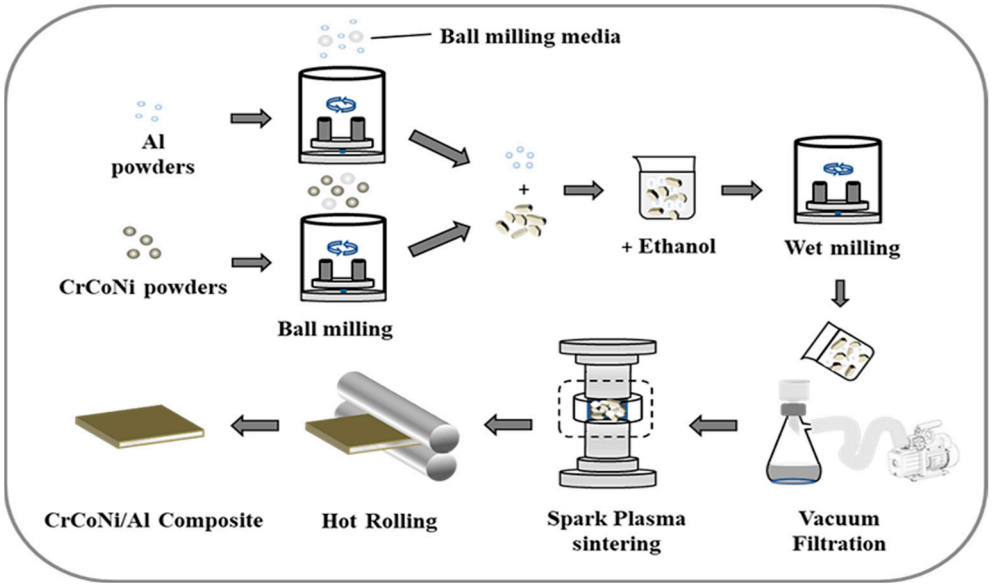

Figure 1. The schematic diagram of the fabrication processes of the CrCoNi/Al composites.

2.2. Microstructural and Mechanical Properties' Characterization

A scanning electron microscope (SEM, FEI Nova Nano230, Sydney, Australia) was used to characterize the morphology of the original powders and the dispersion state of the CrCoNi particles in the fabricated composites. The Cu-Kα radiation source (λ = 0.15406 nm, working voltage of 40 kV, current of 40 mA) of the X-ray diffraction (XRD, Ultima IV, Austin, TX, USA) was employed to identify the phase composition of the composites. The microstructure of the composite was further characterized by a transmission electron

microscope (TEM, TEOL-2100F, Singapore). Prior to the TEM characterization, the sample sheets were firstly ground to 50~60 μm with sandpaper, and were further ion-thinned using the Gatan precision ion polishing system.

The hardness of the composites was characterized using a HDX-1000 TMC microhardness tester. A wire cut electrical discharge machine was used to prepare the compression samples with a size of $3 \times 3 \times 5$ mm^3, and the compression tests at room temperature were performed with an initial compression speed of 1.0 mm/min on the Instron3369 universal testing machine. The averaged compressive yield strength of each type of composite was obtained by three independent tests. The reduced Young's modulus was measured by the TI950 TRIBO nanoindentation with a Berkovich indenter. During the nanoindentation measurement, 20 load-unload circles were used until they reached the max load of 80 mN, and the exerted force was subsequently unloaded without a holding time. The recorded Young's modulus is obtained based on the Oliver–Pharr model [40] and averaged from the measured values of 15 independent tests.

In order to explore the effect of the CrCoNi content on the friction and wear behavior of the composites, a multi-function friction tester (MFT-5000, Rtec-Instruments Inc. San Jose, CA, USA) was used to carry out the reciprocating friction experiments (5 N, 5 Hz, 30 min) with the friction pair of Al_2O_3 balls. The 3D topographies of the wear scar were photographed after testing, and the wear rate was calculated with the Gwyddion software. The SEM was used to observe the surface morphologies of the wear scar and the wear debris, and the wear mechanism were deeply analyzed by the XPS results of the wear scar surface.

3. Results

3.1. Microstructure Observations of the Powders and the Fabricated Composites

Figure 2 shows the SEM images of the original Al powder, CrCoNi powder and the mixed powders. From Figure 2a,b, it can be seen that the Al powder and the original CrCoNi powder both have a spherical shape and a broad size range. Following the ball-milling, the particle size of the Al powder was slightly refined, and the CrCoNi powder successfully changed from a spherical shape to a flake shape.

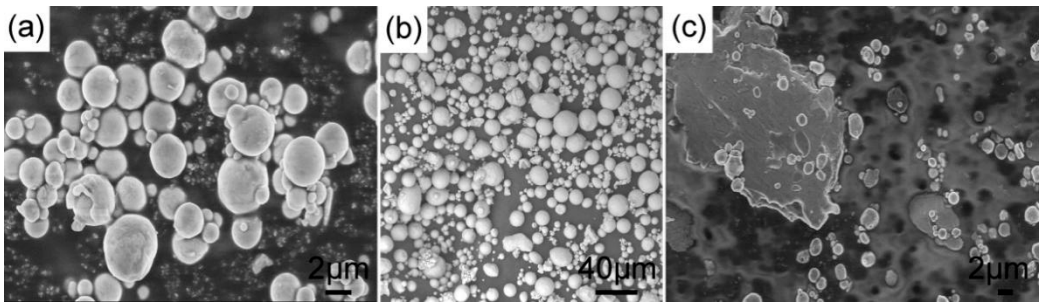

Figure 2. SEM images that reveal the powder morphologies and sizes. (**a**) the raw Al powder; (**b**) the raw CrCoNi powder; (**c**) the mixed Al and CrCoNi powders.

Figure 3 shows the XRD results of the fabricated composites. Four samples with a different CrCoNi content were characterized. It can be seen that the four types of composites have similar diffraction peaks. In addition to Al and CrCoNi, the diffraction peaks belonging to the intermetallic compounds (such as $Al_{0.983}Cr_{0.017}$, $Al_{13}Cr_2$, Co_2A_{l9}, etc.), can also be detected in the diffraction patterns, and the peak intensity increases with the increasing the CrCoNi content. Such a phenomenon indicates that during the bulk composites preparation process, intermetallics have been formed through the limited elemental interdiffusion between the Al matrix and the CrCoNi reinforcement, to some extent, which can provide a good metallurgical bond.

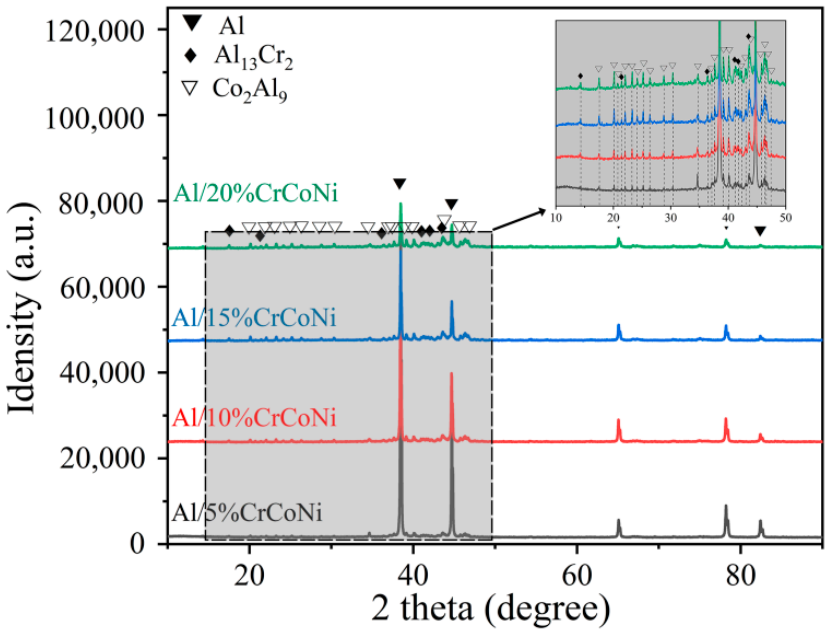

Figure 3. XRD pattern of the CrCoNi MEA reinforced Al matrix composites.

Figure 4 shows the SEM images of the bulk samples, along with the rolling direction. The CrCoNi phase and Al matrix present a white and gray contrast, in these SEM images. As can be seen, there are no residual pores in these bulk composites, indicating that the full densification was achieved after the hot pressing sintering and hot-rolling. Moreover, the dispersion state of the CrCoNi phase varies along with the increasing CrCoNi content. In the composites containing 5 wt.% and 10 wt.% CrCoNi (Figure 4a,b), the CrCoNi particles are singly dispersed in the whole Al matrix, exhibiting a uniform dispersion. By increasing the CrCoNi content to 15 vol.% and 20 wt.% (Figure 4c,d), the CrCoNi particles agglomeration can be observed in the Al matrix. The formation of the CrCoNi clusters would largely deteriorate the mechanical properties of the fabricated composites.

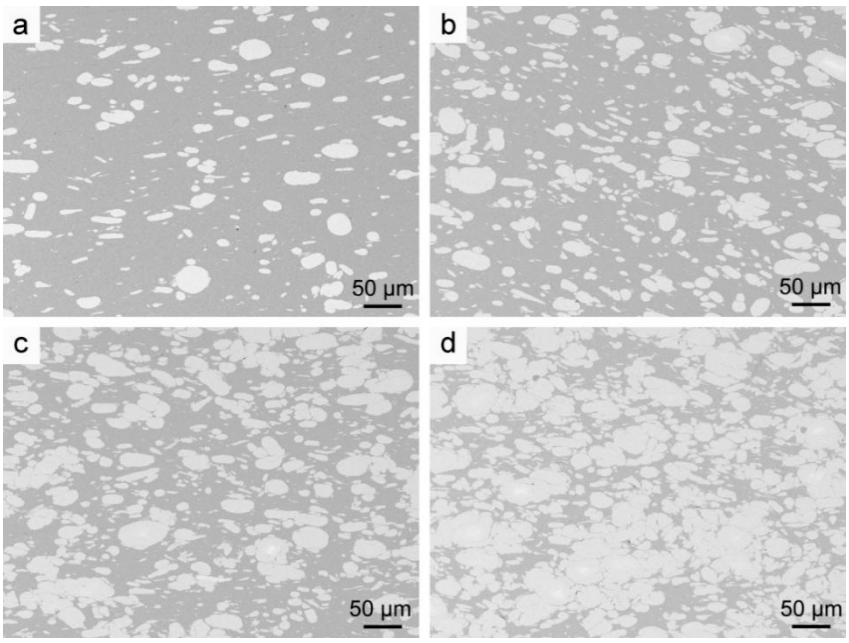

Figure 4. SEM images of the fabricated CrCoNi/Al composites. (**a**) 5 wt.% CrCoNi/Al; (**b**) 10 wt.% CrCoNi/Al; (**c**) 15 wt.% CrCoNi/Al; (**d**) 20 wt.% CrCoNi/Al.

Figure 5 shows the element mapping distribution and the line scanning results acquired from the 5 wt.% CrCoNi reinforced Al matrix composite. As can be seen from Figure 5b, the interdiffusion of Al and Cr, Co and Ni occurred during the composite fabrication processes, according to the line scanning results (Figure 5c). The red dashed line in Figure 5a can further justify the phenomenon of the elements interdiffusion. It can be seen from the line scanning result (Figure 5c) that the Al content gradually decreases from ~90% to ~40% from the Al matrix side to the CrCoNi side, while the content of Cr, Co, and Ni increases from ~3% to ~20%, further demonstrating that the elements of interdiffusion between the Al matrix and CrCoNi particles occurred during the composite fabrication processes. Such an element interdiffusion proved the formation of the metallurgical bonding interface, which can help improve the load transfer efficiency across the interface.

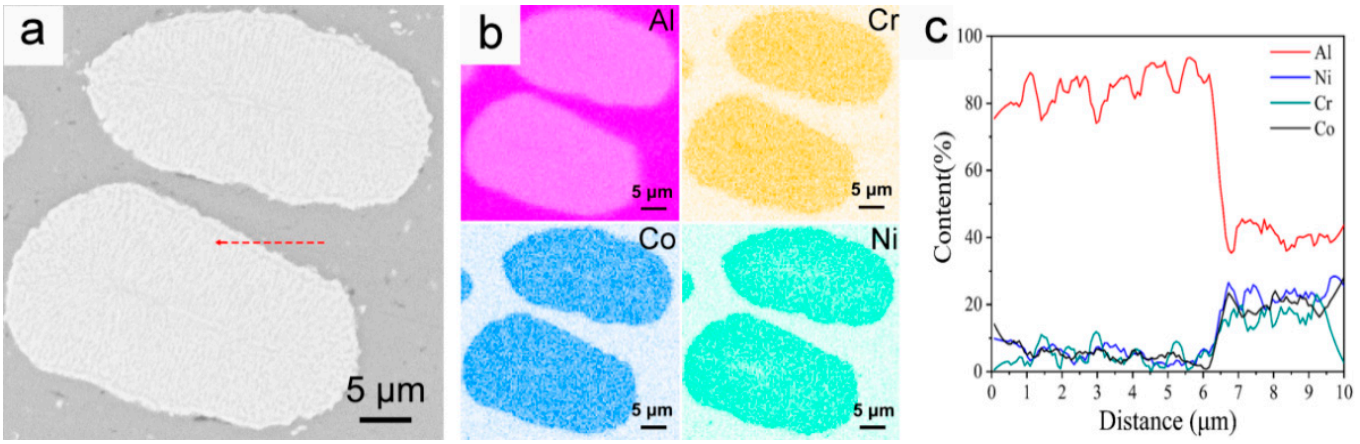

Figure 5. Element distribution around the CrCoNi particles for the 5 wt.% CrCoNi/Al composite. (**a**) SEM image of the selected region, (**b**) elemental mapping images, (**c**) line scanning results (the line scanning track was shown by the red dashed arrow in (**a**)).

Figure 6 shows the TEM image of the interfacial region in the Al-10 wt.% CrCoNi composite. It can be seen from the bright field TEM image (Figure 6a) that the discontinuous particles embedded in the Al matrix, can be attributed to the element diffusion. Figure 6b shows the element mapping results of the red dashed rectangle region in Figure 6a, indicating that the Al element exists in the whole region, the Co and Ni elements have the same distribution position, while the position of the Cr element is not consistent with them. The element distribution was further analyzed by point analyzation, as shown in Figure 6c. According to the element analyzation results, it can be determined that two different types of particles were formed in the interfacial region, one consisting of the Al and Cr elements, and another one containing the Al, Co and Ni elements. Based on the observations, it can be speculated that in the interfacial region of the Cr element in the original CrCoNi particles diffused into the Al matrix caused the original CrCoNi particles to be transformed into the CoNi-rich phase, at the same time, the diffused Cr and CoNi-rich phase reacted with the Al element, resulting in the formation of the Cr-rich and CoNi-rich phases. Figure 6d,e are the high-resolution TEM (HRTEM) images of the two phases, respectively. The interplanar spacing of the Cr-rich phase is 0.341 nm, and the interplanar spacing of the CoNi-rich phase is 0.462 nm. Although the precise crystal structure needs to be further investigated, the crystal structures of the two newly formed phases can be identified as the hcp and fcc structures, respectively, as shown in Figure 6f,g.

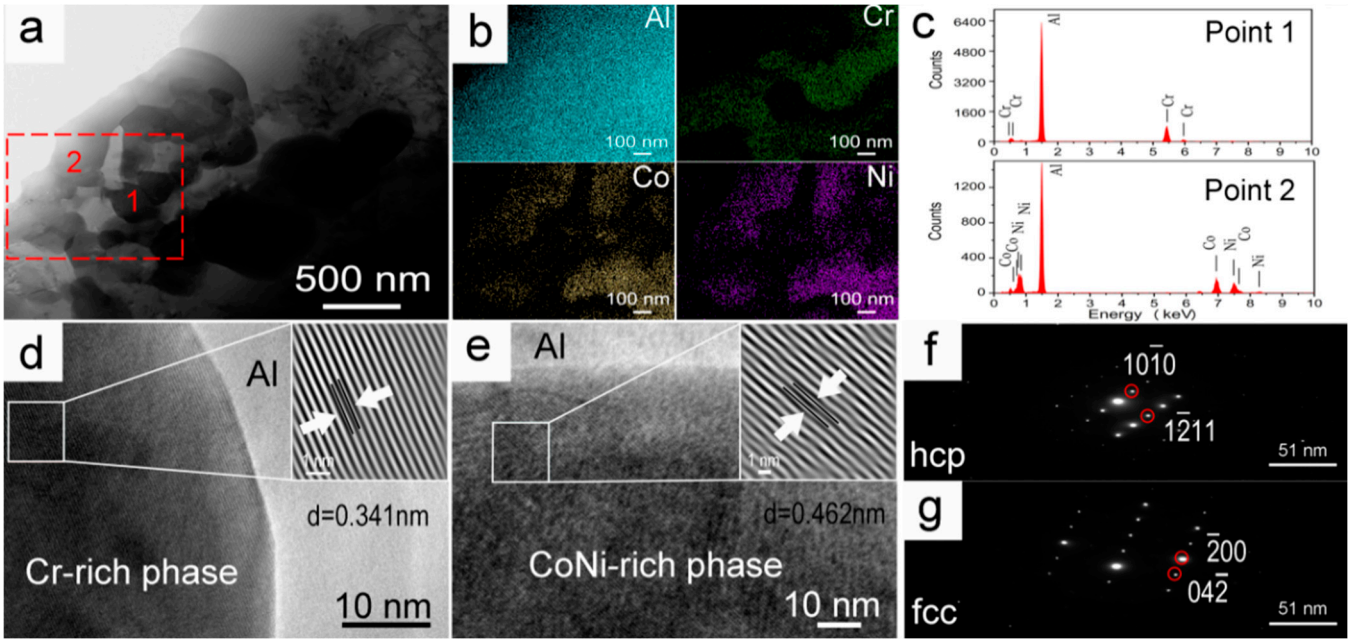

Figure 6. TEM observation of the 10 wt.% CrCoNi/Al composite. (**a**) the bright field TEM image; (**b**) elemental mapping results recorded from the rectangular region in (**a**); (**c**) the EDS results recorded from point 1 and point 2 marked in (**a**); (**d**) HRTEM image of the interface area between the Cr-rich phase and the Al matrix; (**e**) HRTEM image of the interface area between the CoNi-rich phase and the Al matrix; (**f**) SAED pattern acquired from the white rectangular region in (**d**); (**g**) SAED pattern acquired from the white rectangular region in (**e**).

3.2. Mechanical Properties of the Prepared Composites

Figure 7 shows the mechanical properties of the composites with the different CrCoNi content. Figure 7a shows the compressive stress-strain curves of the four types of composites, at room temperature. It can be seen that as the content of the CrCoNi reinforcement increases, the yield strength of the composite increases, but the plasticity of the material decreases at the same time especially, when the CrCoNi content increases to 15 wt.% and 20 wt.%. It is worth noting that the composites with a better plasticity often do not show the characteristics of a brittle failure (cracks occurred in the direction of about 45°–55° to the axis on the surface of the sample) in the compression experiment. With the test proceeding, the cross-sectional area continues to increase at the same time as the flattening of the composites, the pressure-bearing capacity continues to increase, showing a continuously rising compression curve, as shown in the compression stress-strain curve of the 5 wt.% CrCoNi composite (Figure 7a). The composites with 5 wt.% CrCoNi and 10 wt.% CrCoNi have a better plasticity, and the yield strength is as high as 239.27 MPa and 292.24 MPa. Figure 7b shows the comparison of the hardness, yield strength and the compressive strength of the composite. Obviously, as the content of CrCoNi increases, the hardness, the yield strength and the compressive strength all monotonically increase. Figure 7c is the result of the elastic modulus of the composites acquired through the nanoindentation tests. As the content of CrCoNi increases, the modulus of the composite increases from 60.15 GPa to 118.04 GPa, which means the stiffness of the material gradually increases and the plasticity decreases.

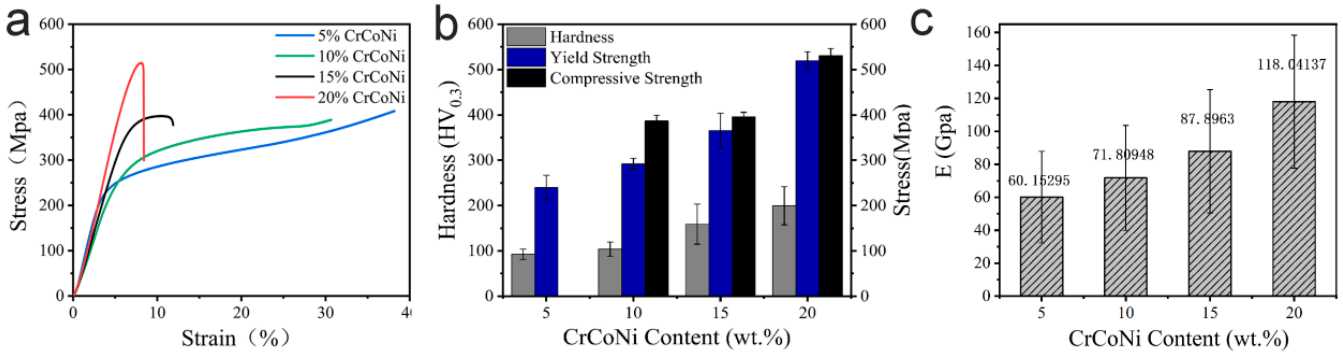

Figure 7. Mechanical properties of the fabricated composites, (**a**) compression stress-strain curves of the composites, (**b**) hardness, compressive strength and yield strength of the composites, (**c**) the elastic modulus results of the composites.

3.3. Tribological Properties of the Composites

Figure 8 shows the friction coefficient curves and the wear rate of the fabricated composites. The same friction condition and parameters were used for each sample (load: 5 N, frequency: 5 Hz, friction time: 30 min, the friction pair: Al_2O_3 grinding balls), and three independent tests were conducted. It can be seen from Figure 8a, that the friction coefficient of the composites with the different CrCoNi content is between 0.4 and 0.5, and shows a downward trend as the content of CrCoNi increases. The wear rate is calculated according to the formula $w = \Delta V/(P \cdot L)$, where ΔV is the wear volume which can be obtained through processing the three-dimensional morphology of the wear scar by the available software, P is the exerted load, and L is the total distance of the friction. As a result, the calculated wear rates of the four types of composites were presented in Figure 8b. It can be clearly seen that the wear rate decreases as the content of CrCoNi increases, indicating CrCoNi is effective in improving the wear resistance of the composites, especially when the content of CrCoNi increases from 10 wt.% to 20 wt.%.

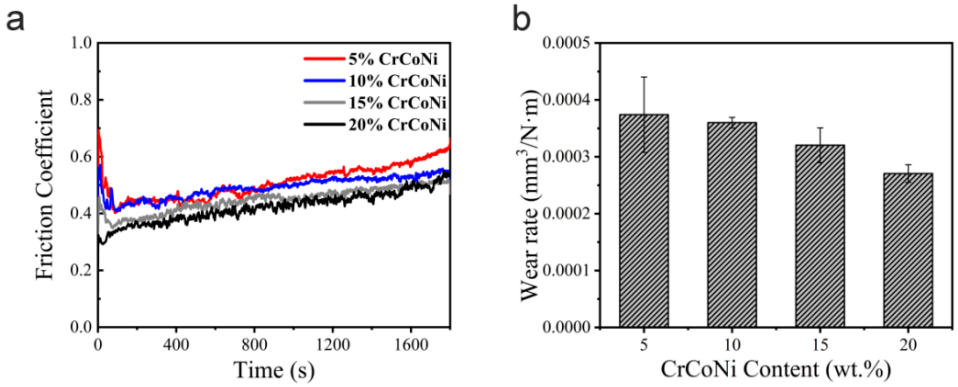

Figure 8. The friction properties of the composites with the different CrCoNi content. (**a**) The coefficient of friction curves of the composites; (**b**) the average wear rate of the composites.

Figure 9 shows the 3D topographies of the wear scar on the surface of the composites after the friction test, the depth profile of the wear scar and the roughness fitting graph of the wear scar in the vertical friction direction. In the 3D topographies of the wear scar (Figure 9a,d,g,j), the deeper color represents a greater depth. It can be found that, as the content of CrCoNi increases, the wear scar becomes shallower, which can be directly evidenced in the depth profile figure (Figure 9b,e,h,k). By increasing the CrCoNi content from 5 wt.% to 10 wt.%, the wear scar depth of the composite is greatly reduced from 75 μm to 55 μm, and the width of the wear scar is also slightly reduced. The 3D topographies of the wear scar and the reduced size of the wear scar profile demonstrate the decrease in the amount of wear, which is consistent with the result of the wear rate. Figure 9c,f,i,l presents

the roughness of the surface of the four composites. Because the roughness at different positions is different, the measured value of the roughness has a certain randomness and is related to the selected position. However, the averaged roughness shows a downward trend. The decrease in the roughness is also in line with the variation trend of the friction coefficient. The fundamental wear mechanism will be further analyzed in the following discussion section.

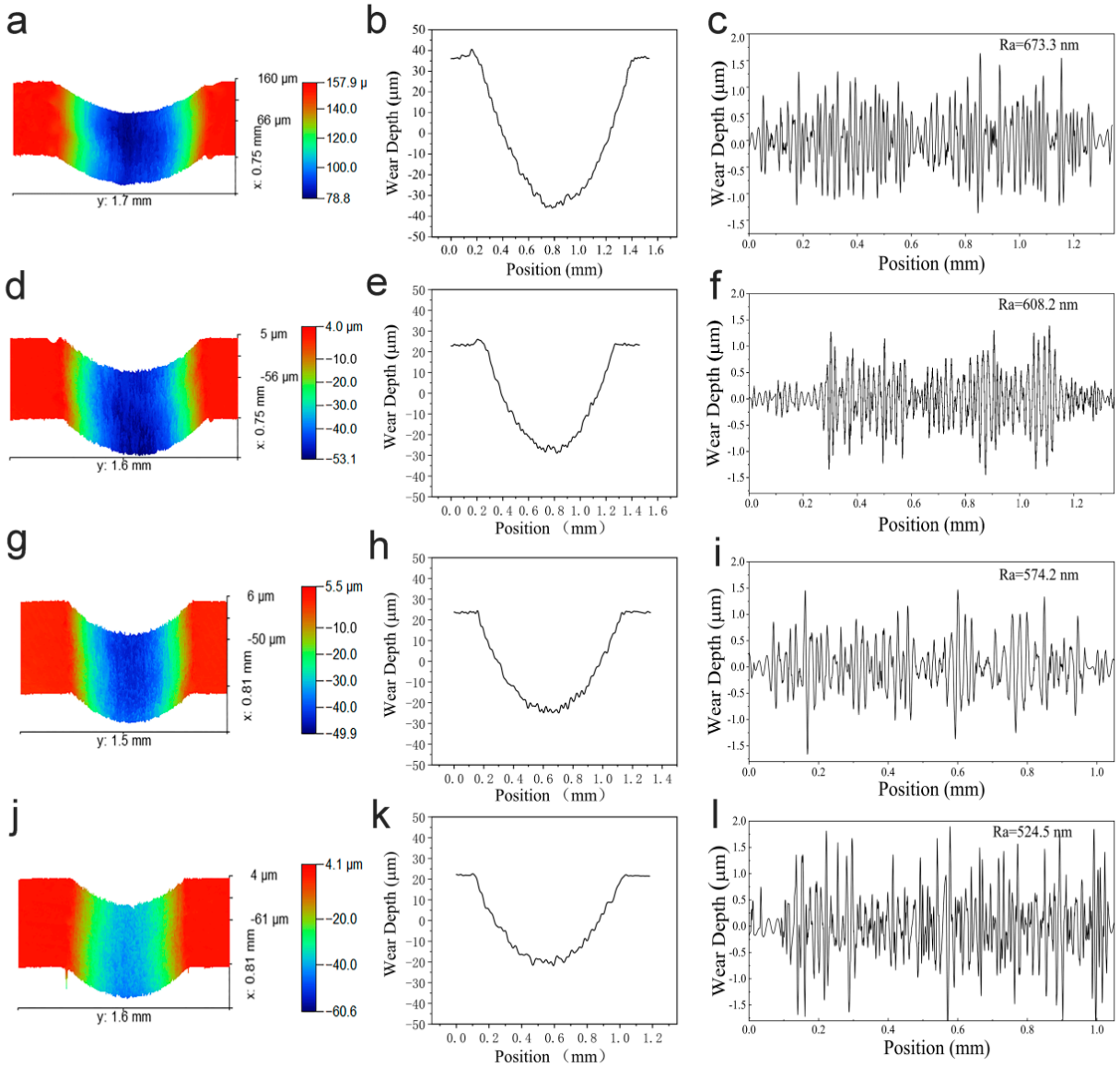

Figure 9. Three-dimensional topographies, the wear scar profiles and the worn surface roughness that are perpendicular to the sliding directions in the Al-5 wt.% CrCoNi composite (**a**–**c**), Al-10 wt.% CrCoNi composite (**d**–**f**), Al-15 wt.% CrCoNi composite (**g**–**i**) and Al-20 wt.% CrCoNi composite (**j**–**l**).

4. Discussion

From the results of the XRD, SEM and TEM, it can be found that the diffusion of elements occurred between the Al matrix and the CrCoNi reinforcements, and the intermetallics even be formed when the CrCoNi content was continuously increased in the composites. Such a phenomenon is consistent with that in the high-entropy alloy particle-reinforced Al matrix composites reported by Liu et al. [29], in which an obvious diffusion transition layer can be detected between the Al matrix and the reinforcement particles. The distinct elements diffusion can be explained in the view of the atomic diffusion behaviors under the present high temperature processing. Owing to the application of pulsing the

current to accelerate the densification processes of the powders during sintering [41,42], a large temperature gradient will be formed from the surface to the core of the particles, after the pulsing current passes through the different particles. Based on the established sintering model by Tan et al. [43], the local high temperature generated around the high-entropy alloy particles enhanced the diffusion reaction. Similar to the high-entropy alloys, there is a large amount of lattice distortion in the CrCoNi MEA, which leads to an increase in the electrical resistivity and a certain difference in the thermal conductivity from the Al matrix. As a result, it can be speculated that the temperature rises sharply at the contact surface of the Al particles and the CrCoNi particles during the quick hot pressing sintering process, with the help of pulsing current. Therefore, the high temperature intensifies the element diffusion at the interface between the Al matrix and the CrCoNi particles, resulting in the formation of the metallurgical bonding interface (as shown in Figure 5), although a relatively low temperature was used in the present study. By increasing the CrCoNi content, many more Al atoms can diffuse into the CrCoNi particles, because the large amount of lattice distortion in the CrCoNi particles provides the "fast channel" for the movement of the Al atoms. At the same time, more Cr atoms can diffuse into the Al matrix, due to its higher diffusion coefficient (6.75×10^{-1} m^2/s), than that of the Co (1.93×10^{-2} m^2/s) and Ni (4.10×10^{-4} m^2/s) atoms in the Al matrix [44]. These diffused Al atoms and Cr atoms can react with the residual Co and Ni atoms in the CrCoNi particles and the Al matrix, respectively, leading to the formation of intermetallics in the interfacial region between the Al matrix and the CrCoNi reinforcements, as demonstrated by the TEM observation on the 10 wt.% CrCoNi/Al composite (Figure 6). Therefore, it can be concluded that the CrCoNi content play a decisive role in the interfacial structure in the prepared CrCoNi/Al composites, when the CrCoNi with a high content was employed as the starting reinforcements, the intermetallics rather than the diffusion of the solid solution would be formed in the interfacial area.

As shown in Figure 5, increasing the CrCoNi content can help achieve a higher strength, hardness, and Young's modulus of the prepared composites, while substantially lowering their ductility at the same time when the CrCoNi content reaches 15 wt.%, which can be mainly attributed to the intensified interfacial reaction. Although the in-situ formation of the intermetallics can strengthen the interfacial bonding between the Al matrix and the CrCoNi particles, thus improving the strength, hardness and Young's modulus of composites, the intrinsic brittleness of the intermetallics frequently decrease the plastic deformation ability of the interfacial region, leading to the deteriorated ductility. As for the 5 wt.% CrCoNi/Al composite, its high combination of strength and ductility can be explained by the limited interfacial interdiffusion between the Al matrix and the CrCoNi composites. The moderate element interdiffusion can improve the interface bonding and avoid the premature failure of the interface during deformation, hence the Al matrix and CrCoNi particles can experience enough hardening work, contributing to a high strength and ductility.

As mentioned earlier, the wear rate and the friction coefficient of the composites decrease with the increasing CrCoNi content, which can be explained by the fundamental wear mechanisms. According to the topography images of the wear scar surface (Figure 10), the distinct plowing grooves and the partial splat pull-out can be seen on the surface of the sample, indicating that the wear process contains an adhesive wear and an abrasive wear. Moreover, it is obvious that with the increase of the CrCoNi content, the splat pull-out and pits of the wear surface on the tested samples gradually decrease, and the wear scar surface becomes smoother. In general, there is a certain correlation between the abrasive wear and the adhesive wear. The abrasive wear is caused by the hard protrusions on the surface of the friction pair, the two surfaces with a certain roughness will adhere to the micro protrusions under the action of the contact pressure at the initial stage of wear. The adhesion points will be sheared under the relative sliding, and then the cracks are formed on the subsurface of the material. Once the cracks propagate, the adhesion points are sheared to form the splat pull-out, pits, delamination and other phenomena [45]. These

flakes form abrasive debris. Some of the softer abrasive debris will be repeatedly crushed by the grinding ball and adhere to the surface of the material. The other hard abrasive debris will form a three-body abrasive wear in the subsequent grinding process, which will cause the plowing groove. Due to the better plasticity of the Al matrix, the greater plastic deformation occurs during the friction process, which increases the actual contact area of the friction pair surface and the wear amount, generating more wear debris and increasing the surface roughness and the friction coefficient. Moreover, the high-hardness CrCoNi reinforcement deforms less compared to the Al matrix and plays a role in supporting and protecting the matrix during the friction process. Therefore, the higher the CrCoNi content, the smaller the deformation that occurs, which means the composite can provide a more effective contacting area and decrease the pressure, and cause the smaller frictional resistance, contributing to the reduction of the amount of wear debris produced and the reduction of the friction coefficient under the same contact pressure [46,47]. Figure 10e is the SEM image of the wear debris of the 5 wt.% CrCoNi/Al sample. Through the EDS point analysis, the wear debris of CrCoNi and the Al matrix can be confirmed and the presence of the oxygen elements was observed, indicating the oxide was formed on the friction surface. Figure 11 shows the XPS results of the wear debris of the 5 wt.% CrCoNi/Al sample. It can be seen that the four elements Al, Cr, Co and Ni all have corresponding oxides, indicating that the present friction is accompanied by the oxidative wear. Among the four elements of Al, Cr, Co and Ni, Al is the most active element, so its oxide occupies the most. The initial oxide film can cover the friction surface and play a certain role of protective effect [48]. When some oxide films with a poor adhesion force fall off, they will also exist in the form of wear debris. The pits formed after falling off increase the surface roughness and aggravate the wear. Therefore, the measured friction coefficient has a slight upward trend and prolongs the friction time.

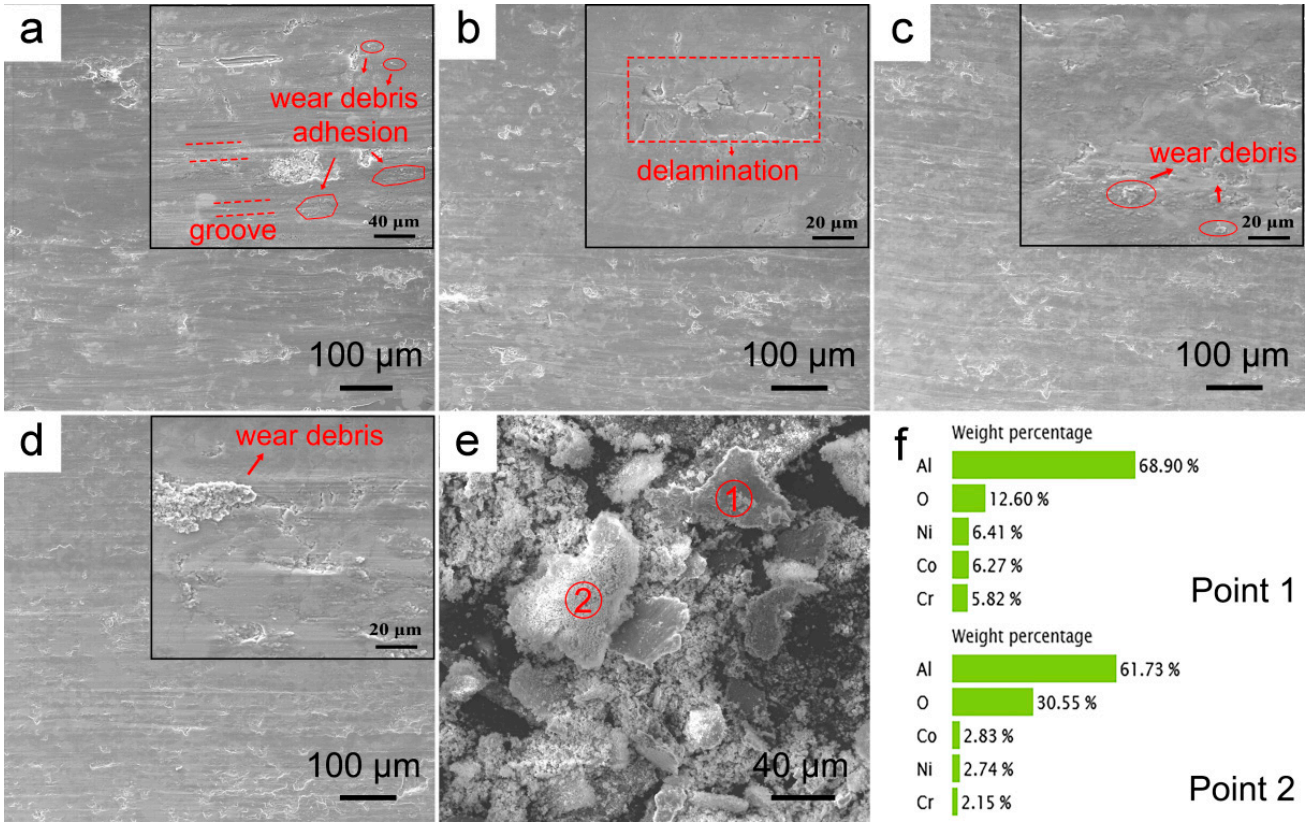

Figure 10. SEM observations of the composites with the different CrCoNi content after friction. (**a**) 5 wt.% CrCoNi; (**b**) 10 wt.% CrCoNi; (**c**)15 wt.% CrCoNi; (**d**) 20 wt.% CrCoNi; (**e**) wear debris of the 10 wt.% CrCoNi/Al composite; (**f**) the EDS results recorded from point 1 and point 2 are marked in (**e**).

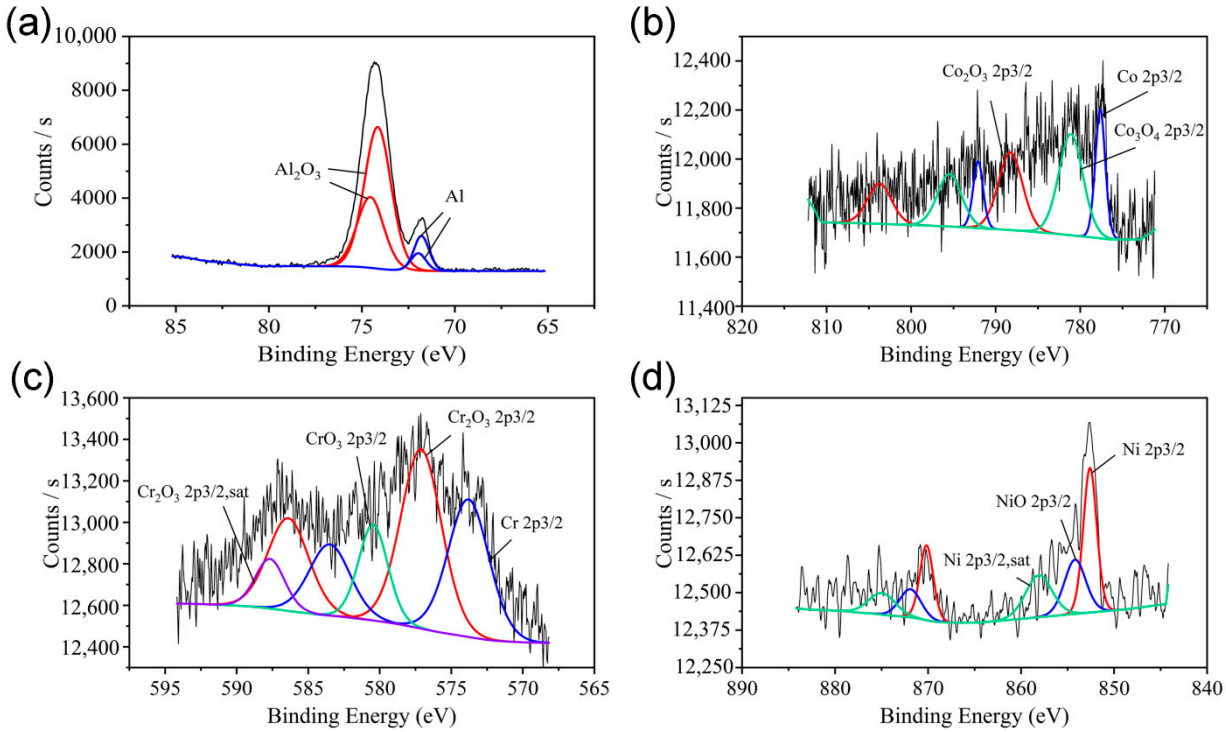

Figure 11. XPS spectra of the worn surfaces of the 5 wt.% CrCoNi/Al composite. (**a**) Al 2p, (**b**) Co 2p, (**c**) Cr 2p, and (**d**) Ni 2p.

In short, it can be concluded that the CrCoNi MEA can substantially strengthen the Al matrix as well as improve its friction resistance, due to the excellent mechanical properties of CrCoNi itself and the proper interfacial bonding with the Al matrix caused by the limited element interdiffusion. Meanwhile, the CrCoNi with a high content (>10 wt.%) promotes the formation of intermetallics, resulting in the substantial decrease of the ductility of the prepared composites.

5. Conclusions

In this study, the novel Al matrix composites reinforced with the CrCoNi MEA particles were prepared thorough the powder metallurgy route, in which the interdiffusion between the Al matrix CrCoNi MEA particles can result in the formation of the metallurgical bonding interface between them, hence contributing to the enhanced mechanical properties and wear resistance. Based on the revealed effects of the CrCoNi content on the microstructures, the mechanical properties and the friction properties of the fabricated composites, the following conclusions can be drawn.

(1) With the usage of the CrCoNi MEA as the starting reinforcement, the mechanical properties of the composites can be highly improved, especially the 5 wt.% CrCoNi/Al composite achieved a high strength without the sacrifice of ductility.

(2) The enhanced strength, hardness, and Young's modulus of the composites can be attributed to the strengthened interfacial bonding between the Al matrix and the CrCoNi reinforcements and the high mechanical performance of the CrCoNi MEA. The ductility of the composites substantially decreases when the content of the CrCoNi MEA exceeds 10 wt.%, due to the formation of the large amounts of intermetallics at the interfacial region.

(3) The wear resistance of the Al matrix composites can be enhanced by the inclusion of the CrCoNi MEA reinforcement, because the CrCoNi MEA can substantially improve the hardness of the composites and promote the formation of the oxidative protection film during the friction process.

Author Contributions: Conceptualization, B.G. and Y.W.; methodology, Y.W. and Z.W.; formal analysis, Y.W. and J.W.; investigation, Y.W., S.L. and Z.Z.; resources, B.G.; data curation, B.G. and Y.W.; writing—original draft preparation, Y.W.; writing—review and editing, B.G. and B.C.; supervision, Z.Y.; project administration, W.L.; funding acquisition, B.G. All authors have read and agreed to the published version of the manuscript.

Funding: This research was funded by the National Natural Science Foundation of China (52004101), the Chinese Postdoctoral Science Foundation (2020T130246), Guangdong Basic and Applied Basic Research Foundation (2020A1515110621), the fund of the state Key Laboratory of Solidification Processing in NWPU (SKLSP202121) and the Fundamental Research Funds for the central Universities (11620345).

Data Availability Statement: The raw/processed data can be provided upon reasonable request.

Conflicts of Interest: The authors declare no conflict of interest.

References

1. Huang, L.; Wang, L.; Qian, M.; Zou, J. High tensile-strength and ductile titanium matrix composites strengthened by TiB nanowires. *Scr. Mater.* **2017**, *141*, 133–137. [CrossRef]
2. Chandran, K.S.R.; Panda, K.B.; Sahay, S.S. TiBw-reinforced Ti composites: Processing, properties, application prospects, and research needs. *JOM* **2004**, *56*, 42–48. [CrossRef]
3. Huang, L.; An, Q.; Geng, L.; Wang, S.; Jiang, S.; Cui, X.; Zhang, R.; Sun, F.; Jiao, Y.; Chen, X.; et al. Multiscale Architecture and Superior High-Temperature Performance of Discontinuously Reinforced Titanium Matrix Composites. *Adv. Mater.* **2020**, *33*, 2000688. [CrossRef]
4. Morsi, K. Titanium–titanium boride composites. *J. Mater. Sci.* **2019**, *54*, 6753–6771. [CrossRef]
5. Zherebtsov, S.; Ozerov, M.; Stepanov, N.; Klimova, M.; Ivanisenko, Y. Effect of High-Pressure Torsion on Structure and Microhardness of Ti/TiB Metal–Matrix Composite. *Metals* **2017**, *7*, 507. [CrossRef]
6. Feng, H.; Zhou, Y.; Jia, D.; Meng, Q.; Rao, J. Growth mechanism of in situ TiB whiskers in spark plasma sintered TiB/Ti metal matrix composites. *Cryst. Growth Des.* **2006**, *6*, 1626–1630. [CrossRef]
7. Wang, X.; Guo, B.; Ni, S.; Yi, J.; Song, M. Acquiring well balanced strength and ductility of Cu/CNTs composites with uniform dispersion of CNTs and strong interfacial bonding. *Mater. Sci. Eng. A* **2018**, *733*, 144–152. [CrossRef]
8. Lu, Q.; Guo, B.; Ni, S.; Yi, J.; Song, M. Preparation. microstructure and properties of Cu-8.3Al/CNTs composites with different volume fractions of CNTs. *Diam. Relat. Mater.* **2020**, *107*, 107912. [CrossRef]
9. Wu, J.; Tang, X.; Zhang, X.; Cen, X.; Guo, B.; Chen, B.; Li, W.; Zhang, Z. Realizing the combination of high strength and good ductility of Cu matrix composites with CrCoNi reinforcement particles and microlaminated structure. *J. Alloys Compd.* **2021**, *872*, 159632. [CrossRef]
10. Guo, B.; Chen, Y.; Wang, Z.; Yi, J.; Ni, S.; Du, Y.; Li, W.; Song, M. Enhancement of strength and ductility by interfacial nano-decoration in carbon nano-tube/aluminum matrix composites. *Carbon* **2020**, *159*, 201–212. [CrossRef]
11. Xu, Q.; Hayes, R.W.; Hunt, W.H.; Lavernia, E.J. Mechanical properties and fracture behavior of layered 6061/SiC p composites produced by spray atomization and co-deposition. *Acta Mater.* **1998**, *47*, 43–53. [CrossRef]
12. Surappa, M.K. Aluminium matrix composites: Challenges and opportunities. *Sadhana* **2003**, *28*, 319–334. [CrossRef]
13. Zheng, R.; Hao, X.; Yuan, Y.; Wang, Z.; Ameyama, K.; Ma, C. Effect of high volume fraction of B4C particles on the microstructure and mechanical properties of aluminum alloy based composites. *J. Alloys Compd.* **2013**, *576*, 291–298. [CrossRef]
14. Manivannan, I.; Ranganathan, S.; Gopalakannan, S.; Suresh, S.; Nagakarthigan, K.; Jubendradass, R. Tribological and surface behavior of silicon carbide reinforced aluminum matrix nanocomposite. *Surf. Interfaces* **2017**, *8*, 127–136. [CrossRef]
15. Devaraju, A.; Kumar, A.; Kumaraswamy, A.; Kotiveerachari, B. Influence of reinforcements (SiC and Al_2O_3) and rotational speed on wear and mechanical properties of aluminum alloy 6061-T6 based surface hybrid composites produced via friction stir processing. *Mater. Des.* **2013**, *51*, 331–341. [CrossRef]
16. Shen, Q.; Wu, C.; Luo, G.; Fang, P.; Li, C.; Wang, Y.; Zhang, L. Microstructure and mechanical properties of Al-7075/B4C composites fabricated by plasma activated sintering. *J. Alloys Compd.* **2014**, *588*, 265–270. [CrossRef]
17. Lu, T.W.; Chen, W.P.; Wang, P.; Mao, M.D.; Liu, Y.X.; Fu, Z.Q. Enhanced mechanical properties and thermo-physical properties of 7075Al hybrid composites reinforced by the mixture of Cr particles and SiCp. *J. Alloys Compd.* **2018**, *735*, 1137–1144. [CrossRef]
18. Lu, T.; Scudino, S.; Chen, W.; Wang, P.; Li, D.; Mao, M.; Kang, L.; Liu, Y.; Fu, Z. The influence of nanocrystalline CoNiFeAl0.4Ti0.6Cr0.5 high-entropy alloy particles addition on microstructure and mechanical properties of SiCp/7075Al composites. *Mater. Sci. Eng. A* **2018**, *726*, 126–136. [CrossRef]
19. Hu, Q.; Zhao, H.; Li, F. Microstructures and properties of SiC particles reinforced aluminum-matrix composites fabricated by vacuum-assisted high pressure die casting. *Mater. Sci. Eng. A* **2017**, *680*, 270–277. [CrossRef]
20. Guo, B.; Song, M.; Yi, J.; Ni, S.; Shen, T.; Du, Y. Improving the mechanical properties of carbon nanotubes reinforced pure aluminum matrix composites by achieving non-equilibrium interface. *Mater. Des.* **2017**, *120*, 56–65. [CrossRef]

21. Guo, B.; Chen, B.; Zhang, X.; Cen, X.; Wang, X.; Song, M.; Ni, S.; Yi, J.; Shen, T.; Du, Y. Exploring the size effects of Al_4C_3 on the mechanical properties and thermal behaviors of Al-based composites reinforced by SiC and carbon nanotubes. *Carbon* **2018**, *135*, 224–235. [CrossRef]
22. Guo, B.; Song, M.; Zhang, X.; Liu, Y.; Cen, X.; Chen, B.; Li, W. Exploiting the synergic strengthening effects of stacking faults in carbon nanotubes reinforced aluminum matrix composites for enhanced mechanical properties. *Compos. Part B Eng.* **2021**, *211*, 108646. [CrossRef]
23. Guo, B.; Zhang, X.; Cen, X.; Chen, B.; Wang, X.; Song, M.; Ni, S.; Yi, J.; Shen, T.; Du, Y. Enhanced mechanical properties of aluminum based composites reinforced by chemically oxidized carbon nanotubes. *Carbon* **2018**, *139*, 459–471. [CrossRef]
24. Zhang, W.W.; Hu, Y.; Wang, Z.; Yang, C.; Zhang, G.Q.; Prashanth, K.G.; Suryanarayana, C. A novel high-strength Al-based nanocomposite reinforced with Ti-based metallic glass nanoparticles produced by powder metallurgy. *Mater. Sci. Eng. A* **2018**, *734*, 34–41. [CrossRef]
25. Yeh, J.W.; Chen, S.K.; Lin, S.J.; Gan, J.Y.; Chin, T.S.; Shun, T.T.; Tsau, C.H.; Chang, S.Y. Nanostructured high-entropy alloys with multiple principal elements: Novel alloy design concepts and outcomes. *Adv. Eng. Mater.* **2004**, *6*, 299–303. [CrossRef]
26. Ye, Y.F.; Wang, Q.; Lu, J.; Liu, C.T.; Yang, Y. High-entropy alloy: Challenges and prospects. *Mater. Today* **2016**, *19*, 349–362. [CrossRef]
27. Yang, X.; Zhang, Y. Prediction of high-entropy stabilized solid-solution in multi-component alloys. *Mater. Chem. Phys.* **2012**, *132*, 233–238. [CrossRef]
28. Cantor, B.; Chang, I.T.H.; Knight, P.; Vincent, A.J.B. Microstructural development in equiatomic multicomponent alloys. *Mater. Sci. Eng. A* **2004**, *375–377*, 213–218. [CrossRef]
29. Liu, Y.; Chen, J.; Li, Z.; Wang, X.; Fan, X.; Liu, J. Formation of transition layer and its effect on mechanical properties of AlCoCrFeNi high-entropy alloy/Al composites. *J. Alloys Compd.* **2019**, *780*, 558–564. [CrossRef]
30. Li, J.; Li, Y.; Wang, F.; Meng, X.; Wan, L.; Dong, Z.; Huang, Y. Friction stir processing of high-entropy alloy reinforced aluminum matrix composites for mechanical properties enhancement. *Mater. Sci. Eng. A* **2020**, *792*, 139755. [CrossRef]
31. Wu, Z.; Bei, H.; Otto, F.; Pharr, G.M.; George, E.P. Recovery, recrystallization, grain growth and phase stability of a family of FCC-structured multi-component equiatomic solid solution alloys. *Intermetallics* **2014**, *46*, 131–140. [CrossRef]
32. Singh, S.; Wanderka, N.; Kiefer, K.; Siemensmeyer, K.; Banhart, J. Effect of decomposition of the Cr-Fe-Co rich phase of AlCoCrCuFeNi high entropy alloy on magnetic properties. *Ultramicroscopy* **2011**, *111*, 619–622. [CrossRef]
33. Guo, S.; Ng, C.; Liu, C.T. Anomalous solidification microstructures in Co-free $Al_xCrCuFeNi_2$ high-entropy alloys. *J. Alloys Compd.* **2013**, *557*, 77–81. [CrossRef]
34. Singh, S.; Wanderka, N.; Murty, B.S.; Glatzel, U.; Banhart, J. Decomposition in multi-component AlCoCrCuFeNi high-entropy alloy. *Acta Mater.* **2011**, *59*, 182–190. [CrossRef]
35. Tang, Z.; Gao, M.C.; Diao, H.; Yang, T.; Liu, J.; Zuo, T.; Zhang, Y.; Lu, Z.; Cheng, Y.; Zhang, Y.; et al. Aluminum Alloying Effects on Lattice Types, Microstructures, and Mechanical Behavior of High-Entropy Alloys Systems. *JOM* **2013**, *65*, 1848–1858. [CrossRef]
36. Wu, Z.; Bei, H.; Pharr, G.M.; George, E.P. Temperature dependence of the mechanical properties of equiatomic solid solution alloys with face-centered cubic crystal structures. *Acta Mater.* **2014**, *81*, 428–441. [CrossRef]
37. Otto, F.; Yang, Y.; Bei, H.; George, E.P. Relative effects of enthalpy and entropy on the phase stability of equiatomic high-entropy alloys. *Acta Mater.* **2013**, *61*, 2628–2638. [CrossRef]
38. Gludovatz, B.; Hohenwarter, A.; Thurston, K.V.; Bei, H.; Wu, Z.; George, E.P.; Ritchie, R.O. Exceptional damage-tolerance of a medium-entropy alloy CrCoNi at cryogenic temperatures. *Nat. Commun.* **2016**, *7*, 10602. [CrossRef] [PubMed]
39. Moravcik, I.; Cizek, J.; Kovacova, Z.; Nejezchlebova, J.; Kitzmantel, M.; Neubauer, E.; Kubena, I.; Hornik, V.; Dlouhy, I. Mechanical and microstructural characterization of powder metallurgy CoCrNi medium entropy alloy. *Mater. Sci. Eng. A* **2017**, *701*, 370–380. [CrossRef]
40. Oliver, W.C.; Pharr, G.M. An improved technique for determining hardness and elastic modulus using load and displacement sensing indentation experiments. *J. Mater. Res.* **1992**, *7*, 1564–1583. [CrossRef]
41. Zhao, S.; Song, X.; Zhang, J.; Liu, X. Effects of scale combination and contact condition of raw powders on SPS sintered near-nanocrystalline WC–Co alloy. *Mater. Sci. Eng. A* **2008**, *473*, 323–329. [CrossRef]
42. Song, X.; Liu, X.; Zhang, J. Neck Formation and Self-Adjusting Mechanism of Neck Growth of Conducting Powders in Spark Plasma Sintering. *J. Am. Ceram. Soc.* **2006**, *89*, 494–500. [CrossRef]
43. Tan, Z.; Wang, L.; Xue, Y.; Zhang, P.; Cao, T.; Cheng, X. High-entropy alloy particle reinforced Al-based amorphous alloy composite with ultrahigh strength prepared by spark plasma sintering. *Mater. Des.* **2016**, *109*, 219–226. [CrossRef]
44. Du, Y.; Chang, Y.A.; Huang, B.; Gong, W.; Jin, Z.; Xu, H.; Yuan, Z.; Liu, Y.; He, Y.; Xie, F.Y. Diffusion coefficients of some solutes in fcc and liquid Al: Critical evaluation and correlation. *Mater. Sci. Eng. A* **2003**, *363*, 140–151. [CrossRef]
45. Ouyang, J.H.; Sasaki, S.; Umeda, K. Low-pressure plasma-sprayed ZrO_2–CaF_2 composite coating for high temperature tribological applications. *Surf. Coat. Technol.* **2001**, *137*, 21–30. [CrossRef]
46. Ye, Y.; Wang, Y.; Wang, C.; Li, J.; Yao, Y. An analysis on tribological performance of CrCN coatings with different carbon contents in seawater. *Tribol. Int.* **2015**, *91*, 131–139. [CrossRef]

47. Al-Samarai, R.A.; Haftirman, K.R.A.; Al-Douri, Y. The influence of roughness on the wear and friction coefficient under dry and lubricated sliding. *Int. J. Sci. Eng. Res* **2012**, *3*, 1–6.
48. Zhiqiang, S.; Di, Z.; Guobin, L. Evaluation of dry sliding wear behavior of silicon particles reinforced aluminum matrix composites. *Mater. Des.* **2005**, *26*, 454–458. [CrossRef]